Time Resolved Thermographic Characterization of Heat Transfer and Fluid Dynamics in Nanofluid Droplets for Cooling Applications

F. M. Matos[1], Q. J. Liang[1], P. Pontes[1], A. S. Moita*[1], A. P. C. Ribeiro[2], A. L. N. Moreira[1]

[1]IN+ Center for Innovation, Technology and Policy Research, Instituto Superior Técnico, Universidade de Lisboa, Av. Rovisco Pais, 1049-001 Lisboa, Portugal

[2]Centro de Química Estrutural, Instituto Superior Técnico, Universidade de Lisboa, Av. Rovisco Pais, 1049-001 Lisboa, Portugal

*Corresponding author: anamoita@tecnico.ulisboa.pt

Abstract

The present work addresses the detailed characterization of the effect of using nanoparticles in the dynamics and heat transfer processes occurring at the impact of nanofluid droplets on a solid heated surface. Gold and silver nanoparticles are dissolved in water DD in concentrations ranging between 0.1wt% and 5wt%. Millimetric droplets with a fixed initial diameter of 3mm are generated and impact on a smooth stainless steel surface with velocities varying between 0.8ms^{-1} and 2ms^{-1}. The surface is heated by Joule effect, from ambient temperature up to 120ºC. Droplet dynamics is evaluated together with the temperature field on the heated surface and with the heat fluxes exchanged during droplet spreading, using synchronized analysis of high-speed video and high-speed thermography. The results show that the heat transfer is indeed enhanced by the presence of the nanoparticles, for low impact velocities (bellow 2ms^{-1}), but is deteriorated as the impact velocity is increased. Detailing the heat transfer vs droplet dynamics for the lowest impact velocities ($V_0=0.8$ms^{-1}) shows that the heat transfer enhancement occurs during the earlier stages of droplet spreading t<20ms, being deteriorated for later stages of spreading 20<t<60ms, even though the spreading diameter of the nanodroplets is larger than that of the water droplet. These results are partially explained by the local increase in the viscosity and in the surface tension of the droplets, as the local concentration of the nanoparticles increases, with water evaporation, but a major role is also expected to be played by wettability. Hence, preliminary results observed with laser scanning confocal microscopy suggest that the nanoparticles tend to deposit on the surface increasing the wettability, at low velocities and for earlier stages of spreading. However, as the nanoparticles concentration increases for later stages of spreading, the particles tend concentrate at the contact line, increasing the local contact angle, which is expected to affect the true wetted area, the flow and the thermal resistance at this region, thus limiting the heat flux that can be transferred from the surface to the droplet.

Keywords
Wettability, droplet dynamics, heat transfer, nanofluids, IR high-speed thermography.

Introduction
The efficient dissipation of high heat loads is a major challenge in many industrial applications such as in microelectronics, solar energy applications and more recently in thermal management in electric vehicles [1-3]. Spray cooling is still pointed as one of the cooling techniques with highest potential, given the large heat transfer coefficients that it can dissipate (of the order of 10^4-10^5 W/m^{2}K) [4]. However, increasingly demanding heat loads are constantly pushing researchers towards the development of more efficient strategies to control and enhance liquid-solid heat transfer processes, which mainly govern the cooling needs for most of the industrial applications. Within this scope, while several authors have attempted to alter surface properties, to enhance the fluid dynamics and heat transfer processes, e.g. [4-6] others focused on the development of innovative fluids with customized enhanced thermophysical properties. In this context, since the pioneering work performed in the 1190s [7], nanofluids have captured the attention of numerous researchers, who reported a wide number of studies in the open literature, devoted to the development of these innovative fluids, with improved thermal properties. Nanofluids are colloidal suspensions of common fluids like water or refrigerants, to which solid nanoparticles, with diameters between 1 and 100 nm are added [7-8]. Despite this extensive research, most of these studies have focused on the use of these fluids in natural and/or forced convection systems, particularly those dealing with liquid phase change [9]. Several others have also focused on the characterization of the thermophysical properties of the nanofluids, although most of them consider the nanofluids as long term stable colloids, with homogeneous bulk properties [10]. This leads to significant discrepancies in the characterization of the properties of the fluids and consequently on the interpretation of the studies. For instance, there are several discrepancies in pool boiling studies regarding the enhancement or deterioration of the heat transfer coefficients and of the critical heat flux, which may be associated to the deposition of the nanoparticles on the heated surfaces, which locally

affect the wettability [7,9]. Regarding the impact of nanofluid sprays and droplets, the research studies reported in the literature are still quite scarce [11-12] and again, many of them focus their interpretation on the potential enhancement of the conductivity of the fluids, leaving possible dynamic and wetting effects to a secondary role. However, recent studies show local changes in the surface tension, which affect the evaporation rate of the droplets. For instance Chen *et al.* [13-14] report that for a critical value of nanoparticles concentration ([13-14] worked with laponite, iron oxide - Fe_2O_3 and silver) the evaporative rates decreased due to the increase in the surface tension and in the latent heat of evaporation of the droplet, resulting from the local increase of nanoparticles concentration, as the liquid evaporates. Consistent results with these findings have also been reported later by Gan and Qiao [15] who addressed the effect of adding alumina (Al_2O_3) nanoparticles on the evaporation of fuel (ethanol-based) droplets.

The aforementioned studies concern the evaporation of suspended droplets and do not address the possible effects of the nanoparticles during droplet/wall interactions. In this context, Sefiane and Bennacer [16] studied the evaporation of water droplets with alumina deposited on PTFE surfaces. [16] show that the depinning of the contact line is slower for the nanofluid droplets, thus their lifetime is larger, but the evaporation is strongly enhanced in the meniscus region due to the wetting dynamics, rather than due to the enhancement of fluid conductivity. On the other hand, the impact of nanofluid droplets on heated surfaces was studied by [17], but the description of the effects of the nanoparticles on droplet dynamics and on the consequent heat transfer processes, was mainly qualitative, as the results suggested that the nanoparticles preclude droplet disintegration and thermal induced atomization. However, [17] refer the need to further investigate the effect of the nanoparticles in droplet dynamics during impact and spreading.

The brief state of the art discussed up to know evidences the need to describe the effect of the nanoparticles in the intricate relation between droplet dynamics and the heat transfer phenomena. This is performed here, combining high-speed visualization with time and spacially resolved infrared (IR) thermography. Hence, droplet dynamics is related to the temperature gradients on the surface during droplet spreading and with the heat fluxes transferred during droplet/wall interactions, for nanofluid droplets impacting on a smooth stainless steel surface. Particular emphasis is given to the potential local effects in wettability, following the results reported in [16-17].

Material and methods
Experimental set-up and working conditions
Gold (Au) and silver (Ag) nanotubes (10-30nm in size), prepared at the Centro de Quimica Estrutural are dissolved in water DD in concentrations ranging between 0.1wt% and 2wt%. 0.5wt% of the surfactant CTAB - Cetyl trimethylammonium bromide is also added to the solution to facilitate the dispersion of the nanoparticles and stabilization of the solutions.

Millimetric droplets with a fixed initial diameter of D_0=3mm are generated in a hypodermic needle and impact on a smooth stainless steel surface with velocities varying between $0.8 \le V_0 \le 2ms^{-1}$. The impact velocity was changed by varying the vertical position of the needle, with reference to the impact surface.

The surface is heated by Joule effect, from ambient temperature up to 120ºC.

The impact surface is a stainless steel foil AISI304, 20 µm thick, 20mm wide and 100mm long, which is heated by Joule effect by applying DC current supplied by a HP6274B DC power supply. The heat flux is continuously imposed, being the temperature controlled by a type K thermocouple. Additional temperature control is performed by monitoring the data provided in real time by the infrared (IR) camera.

Each droplet impacts the surface solely when this shows a uniform and constant temperature value, as checked with the thermal camera.

The heating assembly consists in copper electrodes clamped on the top of the stainless steel foil, which is then glued on the top of an insulating thermal glass. This whole setup is supported on a stainless steel structure, with optical access from the side and from the bottom to obtain the dynamic and thermal behavior of the impacting droplets with high-speed video and thermographic cameras. In this context, the temperature of the surface is monitored from the bottom side of the stainless steel foil, which is black matt painted (spray painted) to increase the emissivity (ε_r=0.95, as provided by the manufacturer). Additional details on the setup are described in [18].

Experimental procedure and measurement uncertainties
The surface is smooth, as variations in the average and in the peak-to-valley roughness, measured with a profilemeter Dektak 3 from Veeco are smaller than 20 nm. Wettability is characterized measuring the quasi-static advancing and receding and the static contact angles, using an optical tensiometer (THETA from Attention). The static contact angle, measured by the sessile drop method was θ=82° ± 1° with water DD, θ=53° ± 1° with water DD + 0.5wt% CTAB + 1wt% Ag and θ=43° ± 1° with water DD + 0.5wt% CTAB + 1wt% Au. Extensive description of the procedures followed to characterize the surface are described, for instance in [6,19]. Adding the nanoparticles and/or the surfactant was not observed to alter the density of the solutions, which was mainly the same as that measured for water (ρ=1000kgm^{-3}@20ºC) using a pycnometer for liquids. Surface tension of the solutions was just slightly lowered from 72.88mNm^{-1}@20ºC (water DD) to 62.9mNm^{-1}@20ºC (water DD + 0.5wt%

CTAB + 1wt% Ag) and to 52.7mNm^{-1}@20ºC (water DD + 0.5wt% CTAB + 1wt% Au). It is worth mentioning that the surface tension was measured with the optical tensiometer (THETA from Attention), using the pendant droplet method. The measurements were performed under controlled ambient conditions of temperature (T=20ºC±3ºC) and relative humidity (HR=99% for measurements accuracy of 2%-5%), so that droplet evaporation was negligible, for the measurement period. More details on the procedures followed to characterize the thermophysical properties of the liquids are described for instance in [20-21]. For the lower concentrations, which will be mainly discussed here, the viscosity of the solutions was also not altered significantly when compared to that of water (μ=1.05mNsm^{-2}@20ºC), either by adding the surfactant or the nanoparticles. For the range of velocities and therefore of shear values tested here, non-Newtonian behaviour was also not detected. However, the detailed rheological analysis of the fluids tested is currently under progress.

The topography and wettability of the impacting surface were carefully checked before and after droplet impact, to assure consistent boundary conditions for each impact event and to control surface cleaning and ageing. Care was also taken to assure that the surface was dry and that the initial surface temperature was reproducible before each droplet impact.

The dynamic behavior of the droplet is recorded by a high-speed camera (Phantom v4.2), which is assembled to take side views of the droplet. The high-speed camera is synchronized with an infrared high speed camera (ONCA-MWIR-InSb from Xenics – ONCA 4696 series), which is placed bellow the heated surface. The frame rate and resolution used were 2200 fps, 512×512px^2 for the high-speed video camera and 1000 fps and 150×150px^2 for the thermographic camera, respectively. The calibration factors, for the arrangements considered here were 100 μm/pixel for the IR arrangement and 40 μm/pixel for the high-speed video arrangement.

Five tests were addressed for each experimental condition, to assure reproducibility of the experiments.

Image post-processing is used to obtain the initial diameter D_0, the impact velocity V_0 and the spreading diameter $D(t)$. Curves of these quantities in time were averaged from at least 3 events taken at similar conditions. The radial temperature profiles were obtained after post processing the IR images using an in-house algorithm, which converts the raw IR images to temperature data. The IR camera was carefully calibrated using a cavity based blackbody radiator device. Calibration and post-processing procedures were custom made to analyze the thermal images, as detailed in [18].

The main uncertainties associated to droplet dynamics and to the heat transfer process occurring at droplet impact and spreading are summarized in Tables 1 and 2, respectively.

Table 1. Uncertainties associated to the main quantities used to describe droplet dynamics. U represents the absolute uncertainty and u is associated to relative uncertainties.

Quantity	Uncertainties U (absolute) or u (relative)
Initial droplet diameter D_o [mm]	$U_{D_o} = \pm 160 \mu m$
Spreading diameter $D(t)$ [mm]	$U_D = \pm 160 \mu m$
Spreading factor $\beta = D(t)/D_o$ [-]	$u_{D/D_o} max = \pm 37\%$ at $(D(t)/D_o = 0.17)$
	$u_{D/D\_o} mim = \pm 7\%$ at $(D/D_o = 3.86)$
Impact velocity U_{V0} [ms^{-1}]	$U_{V0}=0.08ms^{-1}$

Table 2. Uncertainties associated to the main quantities used to describe the heat transfer processes during droplet spreading. U represents the absolute uncertainty and u is associated to relative uncertainties.

Parameter	Uncertainties U (absolute) or u (relative)
Temperature T[K]	$U_T = \pm 1K$
Temperature difference ΔT [K]	$U_{\Delta T} = \pm 1.4K$
	$u_{\Delta T} max = \pm 14\%$ at $(\Delta T = 10\ K)$
	$u_{\Delta T} min = \pm 1.7\%$ at $(\Delta T = 78\ K)$
Imposed volumetric heat flux q''' [Wm^{-3}]	$uq''' max = \pm 12\%$ at $(q''' = 6.5 \cdot 10^6\ [W/m^3])$
Radial distance r [mm]	$U_r = \pm 200\ \mu m$

Results and discussion

High-speed video images were taken to the side view of the impacting droplets, synchronized with bottom view thermal images of the heated thin foil.

The first set of results, depicted in Figure 1, shows the temperature variation along droplet radius, for the nanofluid droplets, taken at different instants after impact. Water is used for comparison as the reference base fluid. In the Figure, r=0mm corresponds to the impact point of the droplet, where the minimum temperatures are

obtained. The surface temperature then tends to increase, as one approaches the rim of the lamella, i.e. for larger radius values [18]. Such temperature profiles were taken for numerous time instants after droplet impact. Here, the profiles obtained for t=8ms, 16ms and 32ms after impact, are shown, for illustrative purposes. The initial surface temperature is 120ºC, which is above saturation, but still is not high enough to promote boiling, since the so-called contact temperature, as defined by Seki [19], $T_c = \frac{\beta_w T_w + \beta_l T_l}{\beta_w + \beta_l}$, where T_W and T_l are the temperatures of the surface and of the liquid and β_W and β_l are their respective effusivities, is not high enough to trigger the boiling of the lamella [20-21].

The surface temperature obtained along the radius of the nanofluid droplets is globally lower for the nanofluid droplets, for the lowest impact velocity V_0=0.8ms^{-1} (Figure 1a). However, this cooling enhancement is not so clear for larger impact velocities (V_0=2ms^{-1}) as shown in Figure 1b). This behaviour is similar for both nanofluids, i.e. either using Au (1wt%) or Ag (1wt%). Actually, for this higher impact velocity, the surface temperature is higher during the spreading of the nanofluid droplets, as compared to the temperature profiles obtained for the surface under the water droplet. This, behaviour, which was consistently observed at various initial surface temperatures, namely $T_{W,0}$=80ºC, 100ºC and 120ºC suggests that cooling enhancement that may be promoted by the use of nanoparticles is supressed for larger impacting and consequently spreading velocities.

The characteristic time scale of droplet spreading (of the order of tens of milliseconds) is too short to observe significant evaporative effects, but qualitative evaluation of droplet shape suggests a faster recoiling and "shrinkage" in droplet diameter, which seems to be associated to a faster evaporation. However, the total lifetime of the nanofluid droplets is actually larger than that of the water droplet. This apparently contrasting behaviour is in agreement with that reported by Chen *et al.* [13-14] on suspended nanodroplets, who actually report an increase in the surface tension of the droplet and in the latent heat of evaporation, as the local nanoparticles concentration increased from less than 0.2% to 1%, which is actually the concentration used in this set of results. Consistently, Sefiane and Bennacer [16] reported and enhancement in the heat transfer near the meniscus, but report an overall slower depinning and longer lifetime for nanofluid droplets.
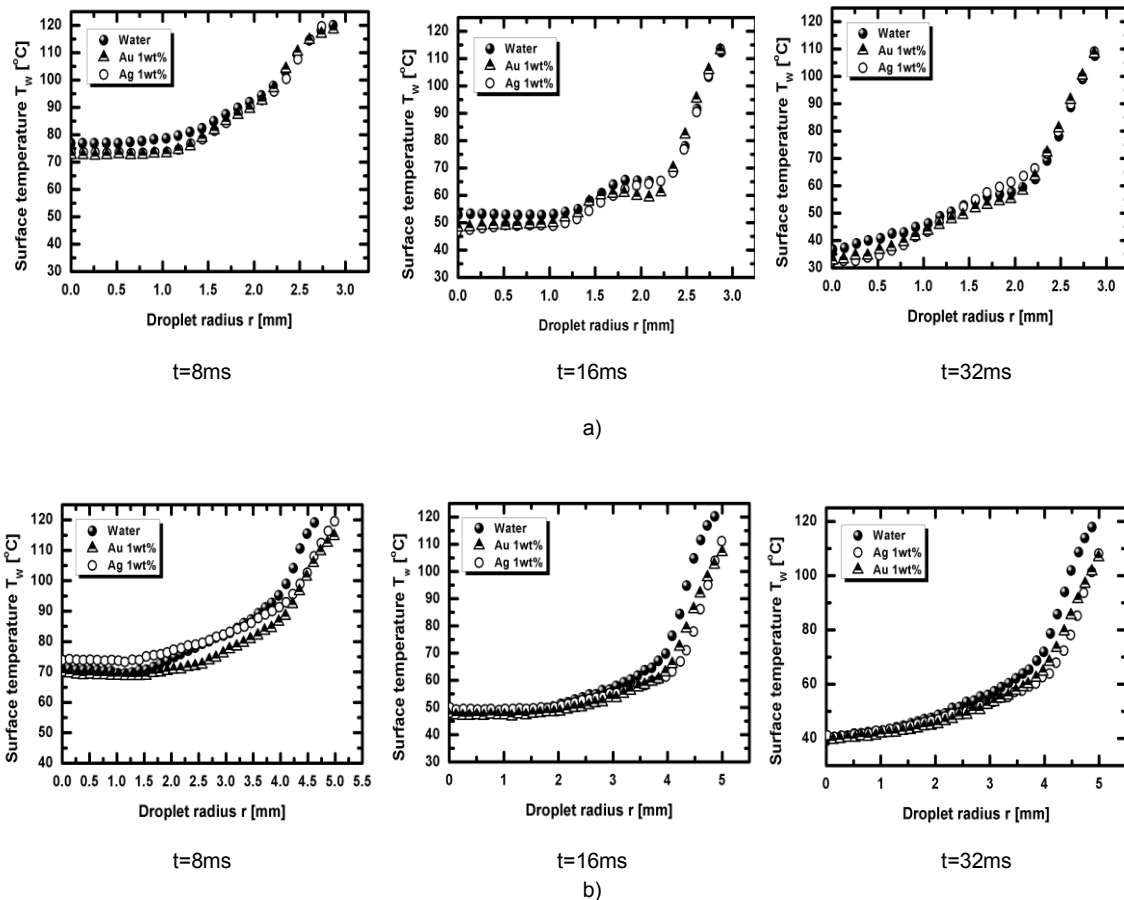
Figure 1. Temperature profiles taken along the radius of water and nanofluids droplets impacting on a smooth and hydrophilic stainless steel surface, initially heated at $T_{W,0}$= 120ºC. The profiles were taken at t=8ms after impact. a) U_0=0.8m/s; b) U_0=2m/s.

Figure 2 depicts the heat flux variation along droplet radius, for various time instants after droplet impact. The initial surface temperature is $T_{W,0}$=120ºC and the nanoparticles concentration was fixed at 1wt%.

One may divide this analysis in two main time intervals; i) an initial time interval, up to t<20ms, corresponding to the period during which the droplet is spreading and receding, i.e. droplet dynamics is still dominant (Figure 2a) and ii) a second period ranging between 20<t<60ms, for which the droplet is approaching its equilibrium state and evaporative effects become more important (Figure 2b).

The plots show significant differences between water and nanofluid droplets for each of these periods. Hence, while in the dynamic period and consistently to the temperature profiles depicted in Figure 1, nanofluid droplets are able to remove slightly larger heat fluxes from the surface, in comparison to the water droplet, for the later stages of spreading the heat fluxes are much similar in terms of absolute magnitude and the water droplet actually is able to remove locally higher heat fluxes. This is particularly evident in the peak of heat flux near the rim (around r=2mm), which is typically observed due to the large temperature gradients generated by the sudden variation of the thickness of the lamella [18]. The rim formation is almost inexistent in the nanofluid droplets, which explains the absence of peaks in the heat flux transferred between the nanofluid droplets and the heated surface (Figure 2b). Hence, while in the earlier stages of spreading, the improved physicochemical properties of the nanofluid droplets allied to the larger spreading diameter (Figure 3a) may explain the higher heat fluxes observed in the nanofluid droplets, for later stages of spreading the heat flux is reduced for the nanofluid droplets, which is not compensated by their larger spreading area, when compared to the water droplet.

Consistently, the cooling efficiency, as a function of the non-dimensional time $t^*=tV_0/D_0$, as defined by Pasendideh-Fard *et al.* [22]:

$$\varepsilon = \frac{\int_t \int_A q^{"} dA dt}{\left(m C_p \Delta T\right)_{water}}$$

(1)

is slightly higher for the nanofluid droplets for $t^*<4$, i.e. during droplet spreading, becoming much smaller for larger non-dimensional times, as the droplets approach their equilibrium phase (Figure 4). Here ΔT is the difference between the initial surface temperature and the bulk temperature of the droplet (assumed to be at ambient temperature) and C_p is the specific heat of water. The heat flux is determined as in [18].
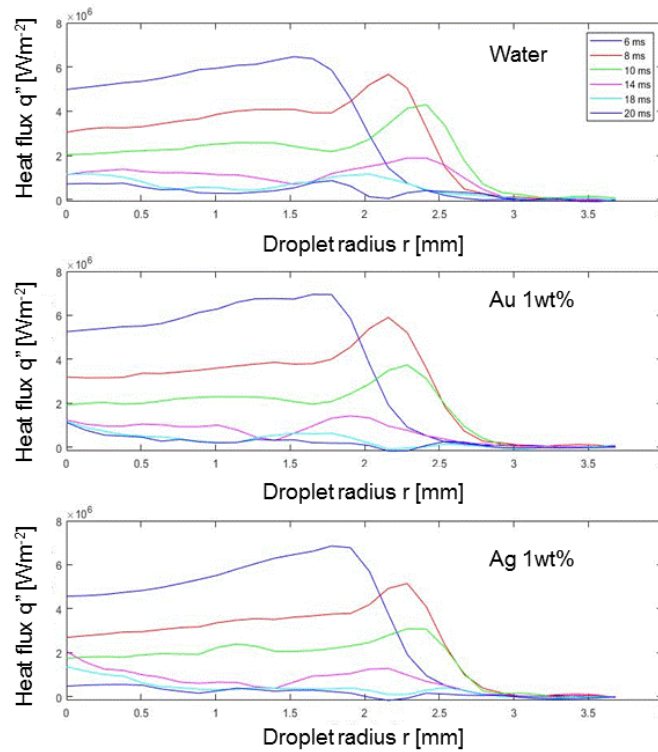
a)
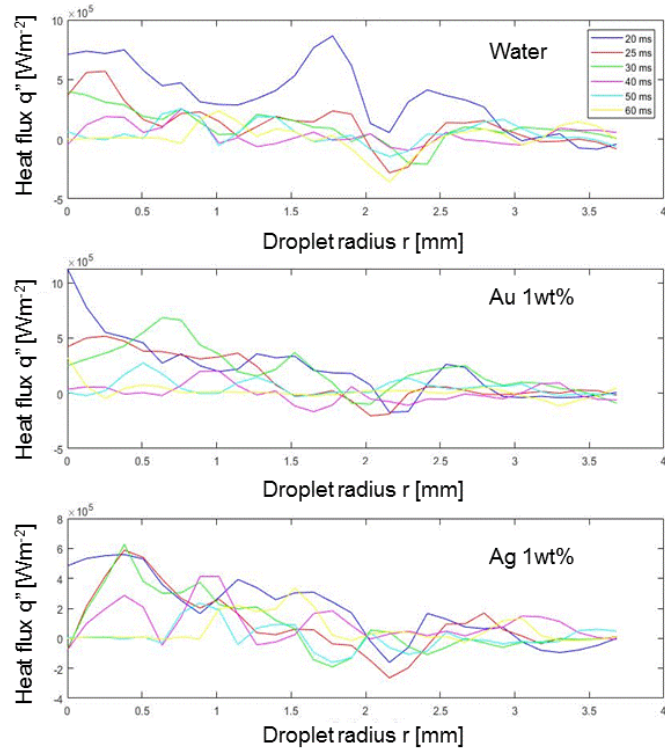
b)

Figure 2. Heat flux along droplet radius, for water and nanofluid droplets impacting a solid smooth and hydrophilic surface heated at $T_{W,0}$=120ºC (D_0=3.0mm, V_0=0.8ms^{-1}).
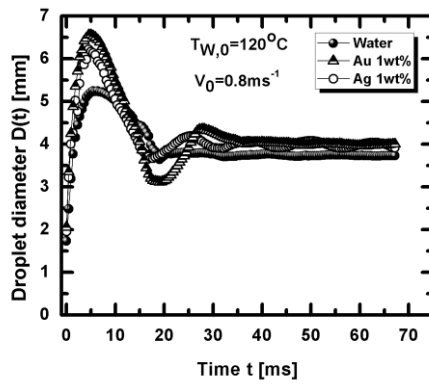
a)
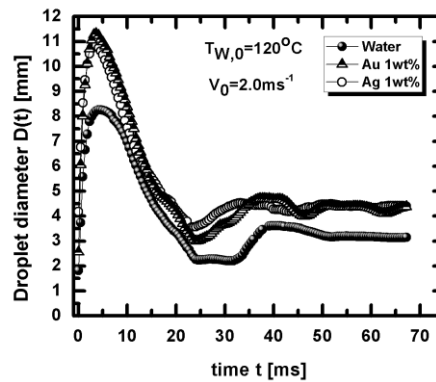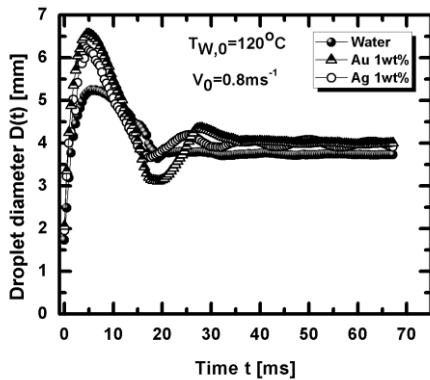
b)
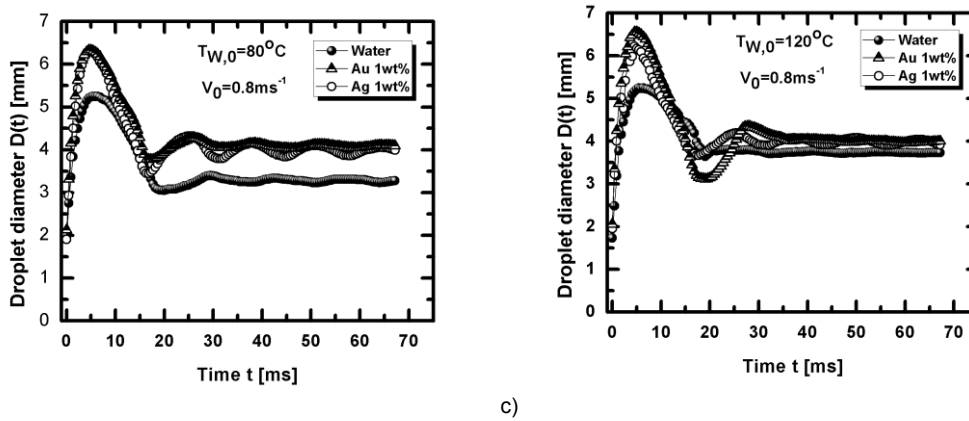
c)

Figure 3. Temporal evolution of the spreading diameter of water and nanofluid droplets on a smooth and hydrophilic stainless steel surface. a) Effect of adding the nanoparticles with a concentration of 1wt% (D_0=3.0mm, V_0=0.8ms^{-1}, $T_{W,0}$=120ºC); b) Effect of the impact velocity on the water and nanofluid droplets (D_0=3.0mm, $T_{W,0}$=120ºC, nanoparticles concentration = 1wt%); c) Effect of the initial surface temperature on the water and nanofluid droplets (D_0=3.0mm, V_0=0.8ms^{-1}, nanoparticles concentration = 1wt%).
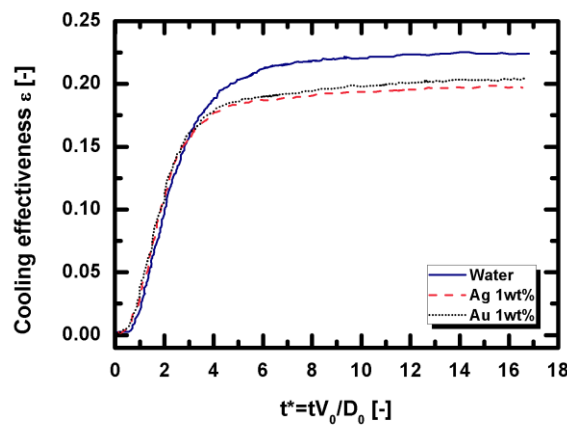
Figure 4. Cooling effectiveness ε as a function of the non-dimensional time $t^*=tV_0/D_0$ for a water and nanofluid droplets impacting on the smooth and hydrophilic, initially heated at $T_{W,0}$ =120ºC.

It is worth mentioning that the nanofluid droplets depict much more oscillations during recoil, when compared to water. This is particularly evident for the nanofluid droplets with gold particles, for the lowest velocity (V_0=0.8ms^{-1}), as shown in Figure 3b). These oscillations are lessened for higher impact velocities. This may be explained by the higher dumping caused by the increased dissipation occurring during spreading, as higher impact velocities lead to larger velocity gradients near the surface. On the other hand, increasing the initial surface temperature from 80ºC to 120ºC promotes these oscillations, particularly for the droplet with silver nanoparticles. This may be associated to the aforementioned local increase of the surface tension during evaporation, as the particles concentration locally increases [13-14]. These first results were obtained for a fixed concentration of the nanoparticles of 1wt%. Different concentrations are now being tested to confirm this trend. However, the small variations in the surface tension cannot totally explain the differences observed here, particularly the heat transfer enhancement which quickly deteriorates as the spreading velocity is increased and/or for later stages of spreading. Hence, this should be associated to local wetting changes. Indeed, preliminary results observed with laser scanning confocal microscopy suggest that the nanoparticles tend to deposit on the surface increasing the wettability, at low velocities. As the velocity and or the concentration increases, the particles tend to migrate to the contact line increasing the local contact angle (which is qualitatively in agreement with the observations reported by [16]). This effect may be influencing the true wetted area, the thermal resistance and the fluid flow near the surface, leading to the worse cooling efficiency of the nanofluid droplets for larger impact velocities and/or later stages of spreading. A deeper analysis is now required, which will be presented in a near future.

Conclusions

This paper focuses on the effect of using nanoparticles in the dynamics and heat transfer processes occurring at the impact of nanofluid droplets on a solid heated surface. The nanofluids are composed by gold and silver nanoparticles, dissolved in water DD, in concentrations ranging between 0.1wt% and 5wt%. The impacting

surface is smooth and is heated from ambient temperature up to 120ºC. Impact velocities range between 0.8ms^{-1} and 2.0ms^{-1} and droplets diameter is fixed at D_0= 3mm.

Droplet dynamics is evaluated together with the temperature field on the heated surface and with the heat fluxes exchanged during droplet spreading, using synchronized analysis of high-speed video and high-speed thermography. The results evidence heat transfer enhancement when using the nanofluid droplets, for earlier stages of spreading (t<20ms) and low impact velocities (V_0=0.8ms^{-1}). Under this scenario, the heat flux is slightly larger for the nanofluid droplets which also depict a larger spreading diameter, when compared to the water droplet. However, for later stages of spreading 20<t<60ms, the heat flux is actually lower and the cooling efficiency is worse for the nanofluid droplets. Any significant improvement is observed when using nanofluid droplets impacting on the surface with higher velocities (V_0=2ms^{-1}). These results can be explained by the slight increase in the surface tension and viscosity in the droplets, as the water evaporates and the nanoparticles concentration locally increases. However, the discrepancies observed at different stages of spreading and different impact velocities should be attributed to variations in the wettability. In this context, preliminary results obtained with laser scanning confocal microscopy suggest a local decrease in the contact angle at earlier stages of spreading due to a small number of particles migration and deposition at the contact line region. However, as the particles concentration in this region increases at later stages of spreading (where evaporation is already relevant) the contact angle seems to increase, which is speculated to decrease the heat flux at this stage, due to the decrease of the true wetted area and increase in the thermal resistance within this region.

Acknowledgements

References

[1] Kim, J., 2007, Int. J. Heat Fluid Flow, 28(4), pp. 753-767.
[2] Mahian O, Kianifar A, Kalogirou S. A., Pop, I. and Wongwises, S. A., 2013, Int. J. Heat Mass Transf., 57, pp. 582-594.
[3] Li, Jiling and Zhu, Z., 2014, "Battery thermal management systems of electric vehicles", Master's Thesis in Automotive Engineering, Charlmers University of Technology, Sweden.
[4] Bostanci H, Daniel R, John K and Louis C., 2009, J Heat Transf., 131, pp. 071401.
[5] Moita, A. S. and Moreira, A. L. N., 2012, Exp, Fluids, 52(3), pp. 679-695.
[6] Moita, A. S., Teodori, E. and Moreira, A. L. N., 2015) Influence of surface topography in the boiling mechanisms. International Journal of Heat and Fluid Flow, 52:50-63
[7] Choi, S.U.S., 1995, ASME FED, 231, pp. 99–105.
[8] Malavasi, I., Teodori, E., Moita, A.S., Moreira, A.L.N. and Marengo, M., 2018, "Wettability effect on pool boiling: a review". Encyclopaedia of Two-Phase Heat Transfer and Flow III: Macro And Micro Flow Boiling And Numerical Modeling Fundamentals (A 4-volume Set), Vol. 4, Edited by J. Thome, World Scientific Publishing Co Pte Ltd. ISBN: 978-981-3227-31-6.
[9] Murshed, S. M. S., Nieto de Castro, C. A., Lourenço, M. J. V., Lopes, M. L. M. and Santos, F. J. V., 2010, Renew. Sust. Energy Rev., 15, pp. 2342–2354.
[10] Murshed,S. M. S., Leong, K. C. and Yang, C., 2008, Appl. Thermal Eng., 28, pp. 2109–2125.
[11] Hsieh, S.-S., Liu, H.-H. and Yeh, Y.-F. Int. J. Heat Mass Transf., pp. 94, pp. 104–18.
[12] Maly, M., Moita, A.S., Jedelsky, J., Ribeiro, A.P.C. and Moreira, A. L. N., 2018, J. Thermal Analysis Calorimetry, (Published online 12 June 2018), pp. 1-12, https://doi.org/10.1007/s10973-018-7444-z
[13] Chen, R.-H., Phuoc, T. X. and Martello, D., 2009, Int. J. Heat Mass Transf., 54, pp. 2459–2466.
[14] Chen, R.-H., Phuoc, T. X. and Martello, D., 2010, Int. J. Heat Mass Transf., 53, pp. 3677–82.
[15] Gan, Y. and Qiao, L., 2011, Int. J. Heat Mass Transf., 54, pp. 4913–4922.
[16] Sefiane, K. and Bennacer, R., 2009, Adv. Coll. Interface Sci., 147–148, pp. 263–271.
[17] Duursma G, Sefiane, K., and Kennedy, A., 2009, Heat Transf. Eng., 30(13), pp. 1108–20.
[18] Teodori, E., Pontes, P., Moita, A.S. and Moreira, A.L.N., 2018, Exp. Thermal Fluid Sci., 96, pp. 284-294.
[19] Pereira P., Moita, A. S., Monteiro, G. and Prazeres, D. M.F., 2014, J. Bionic Eng., 11(3), pp. 346-359.
[20] Moita, A. S., Laurência, C., Ramos, J. A., Prazeres, D. M. F. and Moreira, A.L.N., 2016, J. Bionic Eng., 13(2), pp. 220-234.
[21] Moita, A.S., Vieira, D., Mata, F. and Moreira, A.L.N., 2018, "Microfluidic devices integrating alternative clinical diagnostic techniques based on cell mechanical properties". Biomedical Engineering Systems and Technologies. Series: Comm. Comp. Info. Sci., Chap. 4: Microfluidic Devices Integrating Clinical Alternative Diagnostic Techniques Based on Cell Mechanical Properties, N. Peixoto *et al.* (Eds.), Springer, 881, pp. 74-93.
[20] Cossali, G. E., Marengo, M. and Santini, M., 2005, Proc. 19th ILASS-2005, Orléans, France, pp. 401-406.
[21] Moreira, A. L. N., Moita, A. S. and Panão, M. R., 2010, Prog. Energy Comb Sci. 36, pp. 554-580.
[22] Pasandideh-Fard, M., Aziz, S., Chandra, S. and Mostaghimi, J., 2001, Int. J. Heat Fluid Flow, 22, pp. 201-210.